A Novel Bulk-Flow Model for Improved Predictions of Force Coefficients in Grooved Oil Seals Operating Eccentrically

Luis San Andrés
Mast-Childs Professor
Texas A&M University,
College Station, TX 77843-3123
e-mail: lsanandres@tamu.edu

Adolfo Delgado[1]
GE Research Center,
Niskayuna, NY 12309
e-mail: delgado@ge.com

Oil seals in centrifugal compressors reduce leakage of the process gas into the support bearings and ambient. Under certain operating conditions of speed and pressure, oil seals lock, becoming a source of hydrodynamic instability due to excessively large cross coupled stiffness coefficients. It is a common practice to machine circumferential grooves, breaking the seal land, to isolate shear flow induced film pressures in contiguous lands, and hence reducing the seal cross coupled stiffnesses. Published tests results for oil seal rings shows that an inner land groove, shallow or deep, does not actually reduce the cross-stiffnesses as much as conventional models predict. In addition, the tested grooved oil seals evidenced large added mass coefficients while predictive models, based on classical lubrication theory, neglect fluid inertia effects. This paper introduces a bulk-flow model for groove oil seals operating eccentrically and its solution via the finite element (FE) method. The analysis relies on an effective groove depth, different from the physical depth, which delimits the upper boundary for the squeeze film flow. Predictions of rotordynamic force coefficients are compared to published experimental force coefficients for a smooth land seal and a seal with a single inner groove with depth equaling 15 times the land clearance. The test data represent operation at 10 krpm and 70 bar supply pressure, and four journal eccentricity ratios ($e/c = 0, 0.3, 0.5, 0.7$). Predictions from the current model agree with the test data for operation at the lowest eccentricities ($e/c = 0.3$) with discrepancies increasing at larger journal eccentricities. The new flow model is a significant improvement towards the accurate estimation of grooved seal cross-coupled stiffnesses and added mass coefficients; the latter was previously ignored or largely under predicted. [DOI: 10.1115/1.4004736]

Introduction

Oil seals are used in centrifugal compressors to reduce leakage of the process gas into the oil lubricated bearings as well as into ambient [1,2]. An oil seal, shown in Fig. 1, comprises of a floating ring and elastic support that, under certain operation conditions, may lock up and act as a hydrodynamic journal bearing [2,3]. Oil seals are well known as potential sources of instability due to the generation of large cross-coupled stiffnesses [2–4]. A common practice to minimize the destabilizing effect of oil seals is to machine circumferential grooves to isolate and divide the seal land into separate lands of shorter length, thus reducing the hydrodynamic fluid film forces [5].

To date, there are major discrepancies between predicted and experimental force coefficients obtained for grooved oil seals. Experimental results detailed in Refs. [1,6,7] show that incorporating circumferential grooves does reduce cross-coupled force coefficients but to a lesser extent than predictions otherwise indicate. Furthermore, experimental added mass coefficients are of large magnitude and are not accounted for in available predictive tools [3,4].

Prior art in annular pressure seals considers mainly pump neck ring and interstage seals operating under turbulent flow conditions [8]. The following review discusses the analytical models and experimental results for laminar-flow grooved oil seals, i.e., operating with small axial flow Reynolds numbers, $(\rho V_z c/\mu.) \leq 2000$.

Semanate and San Andrés [3] present an isoviscous bulk-flow analysis to predict force coefficients of grooved oil seals with tapered clearances. The model includes fluid inertia and viscous effects at the seal inlet plane only and considers grooves as uniform pressure sections isolating adjacent lands. Predicted force coefficients, functions of the ring eccentricity, are shown for three configurations with identical land length: single land (smooth), two lands separated by an inner groove, and three lands separated by two inner grooves. Predictions reveal the grooved seals have lesser cross-coupled stiffnesses and direct damping than the single land seal. However, the whirl frequency ratio (WFR), a stability indicator, remains relatively constant at 0.50.

Baheti and Kirk [4] analyze the dynamic forced response of grooved oil seals including thermal effects but neglect fluid inertia within the flow domain. The work includes arched and square grooves at the seal mid-land length. Predictions show a 40% reduction in direct damping and cross-coupled stiffness coefficients when the seal incorporates a square groove with depth to clearance ratio $(d_g/c) = 6$. On the other hand, when using a deeper groove $(d_g/c = 15)$, the seal force coefficients are reduced by a factor of 4 by adding one single groove, and by 10 when adding two inner grooves. The results thus indicate that an inner groove effectively isolates the pressure distribution of contiguous film lands.

Until then, no actual test data was available to verify the predictions; albeit anecdotal evidence pointed out to the effectiveness of the grooving approach to reduce rotordynamic instabilities in centrifugal compressors [5,9].

Childs et al. [1] identify experimentally the dynamic force coefficients and measure the leakage of smooth land and grooved oil seals. The authors aim to quantify the influence of inner-land grooves on the rotordynamic coefficients of oil seals and to

[1]Work conducted as a Research Assistant while at Texas A&M University.

Contributed by the International Gas Turbine Institute (IGTI) of ASME for publication in the Journal of Engineering for Gas Turbines and Power. Manuscript received June 21, 2011; final manuscript received June 22, 2011; published online March 1, 2012. Editor: Dilip R. Ballal.

Copyright © 2012 by ASME

Downloaded 16 Aug 2012 to 165.91.101.108. Redistribution subject to ASME license or copyright; see http://www.asme.org/terms/Terms_Use.cfm

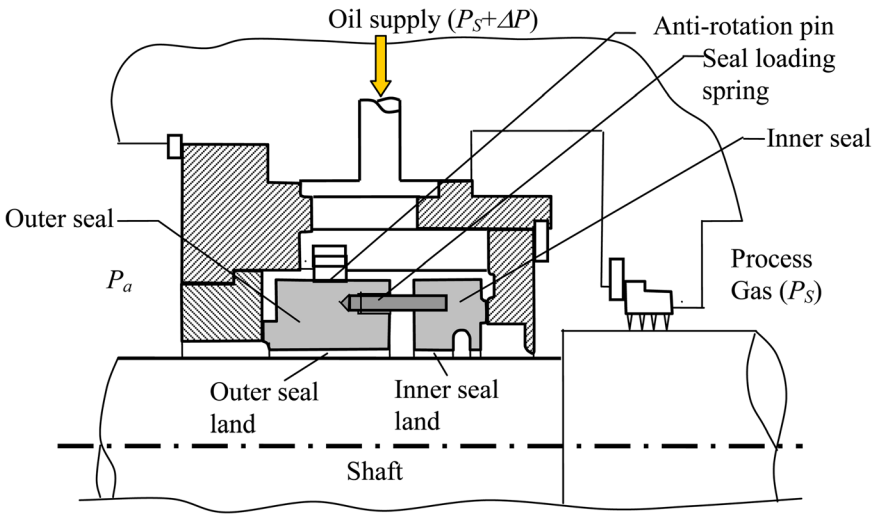

Fig. 1 Typical oil seal multiring assembly

evaluate the accuracy of existing predictive models. Ref. [1] includes a detailed description of smooth and grooved oil seals and their operating features, and a comprehensive literature review. Particularly, the authors note that, prior to their work, the only other published experimental work on laminar flow oil seals was by Kaneko [10], albeit without any grooves. In Ref. [1], static and dynamic force coefficients are identified for a smooth land seal, a one groove seal, and a three groove seal with all groove depths being shallow, $d_g/c=6$. The test force coefficients for the smooth land seal correlate well with predictions from a bulk-flow model [11], except for the added mass coefficient that the analysis underestimates by a factor of about 10. The authors note that the large volume in the oil supply deep groove may explain the large discrepancy. However, pressure measurements at both the supply groove and exit cavity show no dynamic pressure oscillations. The experimental force coefficients for the grooved oil seals are largely underestimated by the model in Ref. [3]. The test results suggest that, contrary to the accepted assumption, inner land grooves are not deep enough to isolate the hydrodynamic pressures from contiguous seal film lands.

Childs et al. [6] present further experimental results evidencing the effect of groove depth on the dynamic force response and leakage of a test oil seal. Force coefficients are identified for four seals: one smooth land seal and three seals with a single groove at the middle of its land with the groove depth increasing as $d_g/c=5$, 10, and 15. The seals force coefficients and leakage are presented versus static journal eccentricity for three rotor speeds and three supply pressures. The experimental force coefficients decrease as the groove depth increases, except for the added mass coefficients. However, predictions derived with the model in Ref. [3] largely underestimate the grooved seal oil cross-coupled stiffnesses and direct damping coefficients even for the test seal with the deepest groove. Thus, the experiments reveal that, even for $d_g/c=15$, a groove does not fully isolate the hydrodynamic pressures of the two adjacent seal lands. For example, the cross-coupled stiffnesses K_{XY} (2 lands) $\neq 1/4$ K_{XY} (1 land), and the direct damping coefficients C_{XX} (2 lands) $\neq 1/4$ C_{XX} (1 land) as predictions readily show. In addition, the experimental results also show relatively large added mass coefficients that (surprisingly) increase as the groove depth increases. However, a prediction of the seal added mass coefficient, derived from a classical formula [12], yields only 2.8 kg, about 10 times smaller than the experimental value!

Hence, the experimental evidence calls for a better predictive model that bridges the gap between theory and practice. Delgado and San Andrés [13][2] introduce a novel bulk-flow analysis, including fluid inertia, for predictions of force coefficients in grooved oils seals and squeeze film dampers operating at their centered position. The model relies on defining an effective groove depth that represents best the physical boundaries of the axial flow through a groove. A parametric study shows predictions agreeing with test force coefficients in Ref. [6] for a narrow range of effective inner groove depths. Specifically, for a short length and shallow groove at the mid-land of an oil seal, predictions of added mass, cross-coupled stiffness, and damping coefficients correlate best with experimental data [6] when using a fraction (typically 50%) of the actual groove depth. Most importantly, the predictions demonstrate that an inner land groove in the oil seal does not isolate the adjacent film lands.

Coinciding with the development in Ref. [13], Gehannin et al. [14] report a comprehensive analysis on the dynamic forced response of SFDs, including the effects of geometric features such as supply orifices, circumferential grooves, end seals, and operating conditions producing oil cavitation. The authors solved numerically bulk flow equations that include convective and temporal fluid inertia effects. The solution of these equations and its implementation to SFDs follows the method introduced by Arghir and Frene [15] for the analysis of turbulent flow liquid annular seals. Predictions in Refs. [14,15] are in good agreement with experimental results obtained in an oil lubricated SFD with a short and shallow feed groove (3 mm $\times$ 3 mm, $d_g/c\sim 15$) and a water lubricated annular seal with multiple short and shallow grooves (1.6 $\times$ 1.6 mm, $d_g/c\sim 15$), respectively.

The current analysis and a prior one [13] stress the significance of an effective depth needed for the bulk-flow model to deliver accurate results, as benchmarked to test data.

Analysis

This paper extends the original analysis in [13] and implements a finite element method to obtain grooved oil seal force coefficient for operation at journal eccentric conditions. The model considers annular cavities with axially symmetric groove configurations, including a central feeding groove, as shown in Fig. 2. This geometry is selected to allow direct comparisons with test data in Ref. [7].

The multiple groove seal is divided into separate flow regions of uniform clearance. In case of a groove, its depth is an effective one (d_η). Ref. [13] fully justifies the rationale for the assumption.

The following derivation applies to each individual flow region with constant clearance, and with a local coordinate system whose origin is at the entrance of a corresponding flow region, grooved or not. Thermal effects are not incorporated in the current analysis; they are not important in high pressure oil seals since the through flow quickly displaces the mechanical energy dissipated

[2]Ref. [13] contains a comprehensive review of the past literature on force coefficients for grooved oil seals and squeeze film dampers.

Downloaded 16 Aug 2012 to 165.91.101.108. Redistribution subject to ASME license or copyright; see http://www.asme.org/terms/Terms_Use.cfm

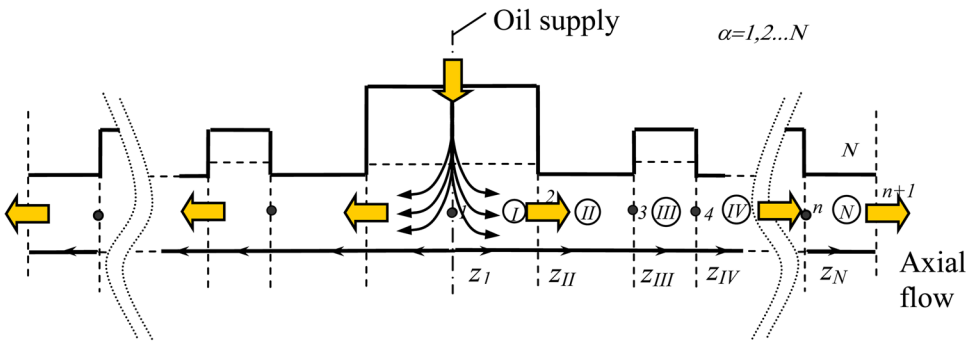

Fig. 2 Schematic view of grooved annular cavity divided into flow regions

and henceforth the lubricant temperature increases little. Figure 3 depicts the journal and the coordinate system used in the analysis for small amplitude journal motions about an off-centered (eccentric) position.

Within each individual flow region the mass flow rates in the circumferential (x) and axial (z) directions are:

$$\dot{m}_{x_\alpha} = \rho\, h_\alpha V_{x_\alpha}, \quad \dot{m}_{z_\alpha} = \rho\, h_\alpha V_{z_\alpha} \quad \alpha=I,II,\ldots N \tag{1}$$

where h_α is the film thickness, $(V_{x_\alpha}, V_{z_\alpha})$ are bulk-flow velocities in each flow region α, and ρ is V, the lubricant density. The bulk-flow continuity and moment transport equations without fluid advection terms are [16]:

$$\frac{\partial}{\partial x}(\dot{m}_{x_\alpha}) + \frac{\partial}{\partial z_\alpha}(\dot{m}_{z_\alpha}) + \frac{\partial}{\partial t}(\rho\, h_\alpha) = 0 \tag{2}$$

$$-h_\alpha \frac{\partial P_\alpha}{\partial x} = 12\,\frac{\mu}{h_\alpha}\left(V_{x_\alpha} - \frac{\Omega R}{2}\right) + \frac{\partial(\dot{m}_{x_\alpha})}{\partial t} \tag{3}$$

$$-h_\alpha \frac{\partial P_\alpha}{\partial z_\alpha} = 12\,\mu\,\frac{V_{z_\alpha}}{h_\alpha} + \frac{\partial(\dot{m}_{z_\alpha})}{\partial t}, \quad \alpha=I,II,\ldots N \tag{4}$$

Above, μ is the lubricant viscosity and P_α is the pressure in each flow region. Eqs. (3) and (4) are rewritten as:

$$\begin{aligned} \dot{m}_{x_\alpha} &= -\frac{\rho\, h_\alpha^3}{12\,\mu}\frac{\partial P_\alpha}{\partial x} - \frac{\rho\, h_\alpha^2}{12\,\mu}\frac{\partial(\dot{m}_{x_\alpha})}{\partial t} + \frac{\rho\, h_\alpha \Omega R}{2} \\ \dot{m}_{z_\alpha} &= -\frac{\rho\, h_\alpha^3}{12\,\mu}\frac{\partial P_\alpha}{\partial z_\alpha} - \frac{\rho\, h_\alpha^2}{12\,\mu}\frac{\partial(\dot{m}_{z_\alpha})}{\partial t}, \quad \alpha=I,II,\ldots N \end{aligned} \tag{5}$$

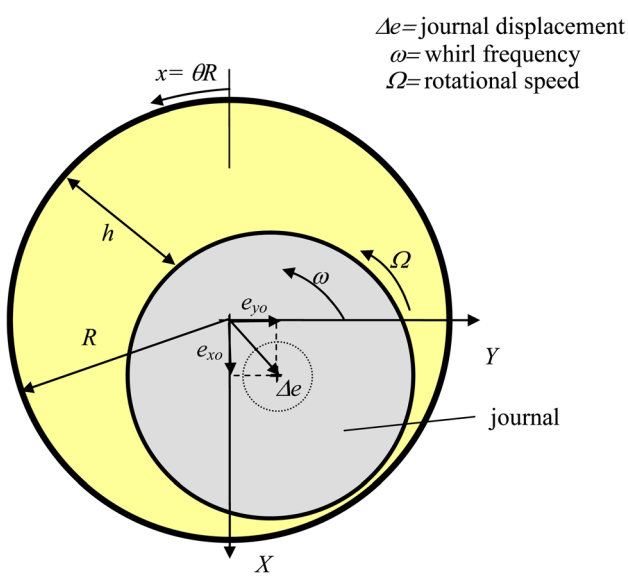

Fig. 3 View of rotating and whirling journal and coordinate system for bulk-flow analysis

Differentiating $\dot{m}_{x_\alpha}$ with respect to x, and $\dot{m}_{z_\alpha}$ with respect to z_α, adding both equations, and disregarding second order terms yields a Reynolds-like equation for the film pressure of an incompressible fluid [16]

$$\frac{\partial}{\partial x}\left(h_\alpha^3 \frac{\partial P_\alpha}{\partial x}\right) + \frac{\partial}{\partial z_\alpha}\left(h_\alpha^3 \frac{\partial P_\alpha}{\partial z_\alpha}\right) = 12\mu\frac{\partial}{\partial t}(h_\alpha) + 6\mu R\Omega\frac{\partial}{\partial x}(h_\alpha) + (\rho h_\alpha^2)\frac{\partial^2}{\partial t^2}(h_\alpha), \quad \alpha=I,II,\ldots N \tag{6}$$

The journal describes whirl motions of small amplitude $(\Delta e_X, \Delta e_Y) \ll c_{\eta_\alpha}$ and frequency ω about the static eccentric position (e_{Xo}, e_{Yo}). The film thickness is

$$\begin{aligned} h_\alpha &= h_{0_\alpha} + e^{i\omega t}\{\Delta e_X \cos(\theta) + \Delta e_Y \sin(\theta)\} \\ &= h_{0_\alpha} + e^{i\omega t}\,\Delta e_\sigma h_\sigma, i = \sqrt{-1}, \sigma = X, Y, \quad \alpha=I,II,\ldots N \end{aligned} \tag{7}$$

with

$$\begin{aligned} h_{0_\alpha} &= c_{\eta_\alpha} + e_X\cos(\theta) + e_Y\sin(\theta) = c_{\eta_\alpha} + e_{\sigma_0} h_\sigma \\ h_X &= \cos(\theta), \quad h_Y = \sin(\theta) \end{aligned} \tag{8}$$

and $c_{\eta_\alpha} = (c + d_{\eta_\alpha})$ is the effective clearance in a groove region.

The pressure is expressed as a superposition of a zero$_{\text{th}}$ order field (P_o) and first order (dynamic) fields $(P_{X_\alpha}, P_{Y_\alpha})$

$$P_\alpha = P_{0_\alpha} + \Delta e_\sigma P_{\sigma_\alpha} e^{i\omega t}, \quad \alpha=I,II,\ldots N \tag{9}$$

Substitution of Eqs. (7) and (9), into Eq. (6) gives the zero$_{\text{th}}$ order equations for the equilibrium pressure,

$$\frac{\partial}{\partial x}\left(h_{0_\alpha}^3 \frac{\partial P_{0_\alpha}}{\partial x}\right) + \frac{\partial}{\partial z_\alpha}\left(h_{0_\alpha}^3 \frac{\partial P_{0_\alpha}}{\partial z_\alpha}\right) = 6\mu R\Omega\frac{\partial}{\partial x}(h_{0_\alpha}) \quad \alpha=I,II,\ldots N \tag{10}$$

and the first order equations for journal dynamic displacements along the X and Y directions,

$$\begin{aligned} &\frac{\partial}{\partial x}\left(h_\alpha^3 \frac{\partial P_{\sigma_\alpha}}{\partial x}\right) + \frac{\partial}{\partial z_\alpha}\left(h_\alpha^3 \frac{\partial P_{\sigma_\alpha}}{\partial z_\alpha}\right) \\ &= 12\,i\,\mu\,\omega\{1 + i\,\overline{\mathrm{Re}}_{*_\alpha}\}h_\sigma + 6\mu\Omega R\frac{dh_\sigma}{dx} \\ &- \frac{\partial}{\partial x}\left(3h_{0_\alpha}^2 h_\sigma \frac{\partial P_{0_\alpha}}{\partial x}\right) - \frac{\partial}{\partial z}\left(3h_{0_\alpha}^2 h_\sigma \frac{\partial P_{0_\alpha}}{\partial z}\right) \quad \sigma=X,Y;\ \alpha=I,II,\ldots N \end{aligned} \tag{11}$$

where $\overline{\mathrm{Re}}_{*_\alpha} = \frac{\rho\omega c_{\eta_\alpha}^2}{12\,\mu}$ is a modified local squeeze film Reynolds number. From the solution of Eq. (10), the fluid film reaction forces at a static journal position (e_{Xo}, e_{Yo}) are

Downloaded 16 Aug 2012 to 165.91.101.108. Redistribution subject to ASME license or copyright; see http://www.asme.org/terms/Terms_Use.cfm

$$\begin{bmatrix} F_{X_0} \\ F_{Y_0} \end{bmatrix} = \sum_{\alpha=1}^{N} \int_0^{L_\alpha} \int_\theta P_{0_\alpha} \begin{bmatrix} \cos\theta \\ \sin\theta \end{bmatrix} R d\theta dz_\alpha \tag{12}$$

After solution of Eqs. (11), the seal force coefficients (stiffness, damping and inertia) are obtained by integrating the dynamic pressure fields over the flow domain [13],

$$K_{\sigma\beta_\alpha} - \omega^2 M_{\sigma\beta_\alpha} + \mathrm{i}\omega C_{\sigma\beta_\alpha} = -\sum_{\alpha=1}^{N} \int_0^{L_\alpha} \int_\theta h_\sigma P_{\beta_\alpha} R d\theta dz_\alpha \quad \sigma,\beta=X,Y;\ \alpha=I,II,\ldots N \tag{13}$$

Finite Element Solution of the Modified Reynolds Equations. Solving the Reynolds-like Eqs. (10) and (11) uses the FEM, as in Ref. [17]. Without loss of generality, the solution is presented for a symmetric oil seal with an inlet groove and a single mid-land groove similar to the seal in Ref. [7]. A similar solution procedure can be applied to other multi-groove seal geometries.

Following the discretization of the domain into elements (Ω^e), see Fig. 4, the static and dynamic pressure fields are represented as the linear combination of nodal values $\bar{P}_i^e$ within each element,

$$P_0^e = \sum_{i=1}^{n_{pe}} \Psi_i \bar{P}_{0_i}^e, \quad P_\sigma^e = \sum_{i=1}^{n_{pe}} \Psi_i \bar{P}_{\sigma_i}^e, \quad \sigma=X,Y \tag{14}$$

where ψ^e are bilinear interpolation functions. The variational or weak forms of Eqs. (10) and (11) using the interpolation functions as weight functions are obtained [17]. For the zero$_{\text{th}}$ order pressure the FE equation is

$$\sum_{j=1}^{n_{pe}} k_{ij}^e \bar{P}_{0_j}^e = -q_i^e + f_i^e \tag{15}$$

with

$$k_{ij}^e = \iint_{\Omega^e} \left(\frac{h_{0_\alpha}^3}{12\mu}\right)^e \left\{\frac{\partial \Psi_i}{\partial x}\frac{\partial \Psi_j}{\partial x} + \frac{\partial \Psi_i}{\partial z}\frac{\partial \Psi_j}{\partial z}\right\}^e dx\,dz \tag{16a}$$

$$f_{0_i}^e = \frac{\Omega R}{2} \iint_{\Omega^e} h_{0_\alpha} \frac{\partial \Psi_i^e}{\partial x} dx\,dz \tag{16b}$$

$$q_{0_i}^e = \oint_{\Gamma^e} \Psi_i^e q_{\eta_0} d\Gamma^e, \text{ with } q_{\eta_0} = -\frac{h_{0_\alpha}^3}{12\mu}\frac{\partial P_0}{\partial n} + \frac{h_{0_\alpha}\Omega R}{2}\eta_x \tag{16c}$$

Similarly for the perturbed pressure fields, P_X and P_Y, the set of equations for the nodal pressures in a finite element are

$$\sum_{j=1}^{n_{pe}} k_{ij}^e \bar{P}_{\sigma_j}^e = f_{\sigma_i}^e - \sum_{j=1}^{n_{pe}} S_{\sigma_{ij}}^e \bar{P}_{0_j}^e - q_{\sigma_i}^e, \quad \sigma=X,Y \tag{17}$$

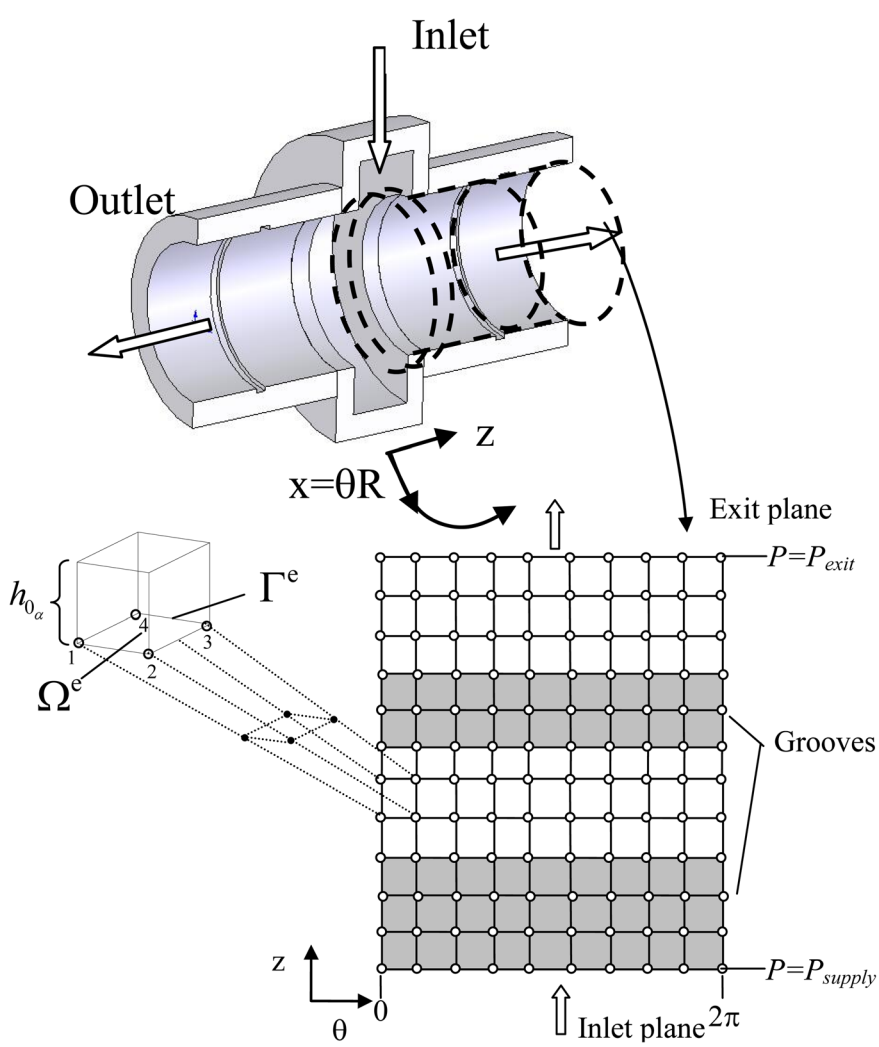

Fig. 4 Coordinate system and sample FE mesh for oil seal model

Downloaded 16 Aug 2012 to 165.91.101.108. Redistribution subject to ASME license or copyright; see http://www.asme.org/terms/Terms_Use.cfm

where

$$f^e_{\sigma_i} = \iint_{\Omega^e} h_\sigma \left[\frac{\Omega R}{2} \frac{\partial \Psi^e_i}{\partial x} + \frac{\rho\,\omega^2}{12\,\mu} \Psi^e_i\, h^2_{0_\alpha} \right] dxdz - \mathbf{i}\,\omega \iint_{\Omega^e} h_\sigma \left[\Psi^e_i \right] dxdz \tag{18a}$$

$$S^e_{\sigma_{ij}} = \iint_{\Omega^e} \left(\frac{3\,h^2_{0_\alpha}}{12\mu} \right)^e \left\{ \frac{\partial \Psi_i}{\partial x}\frac{\partial \Psi_j}{\partial x} + \frac{\partial \Psi_i}{\partial z}\frac{\partial \Psi_j}{\partial z} \right\}^e h_\sigma dxdz \tag{18b}$$

$$f^e_{\sigma_i} = \oint_{\Gamma^e} \Psi^e_i q_{\eta_\sigma} d\Gamma^e \text{ with } q_{\eta_\sigma} = \left(-\frac{h^3_{0_\alpha}}{12\mu}\frac{\partial P_\sigma}{\partial \eta} - \frac{3h^2_{0_\alpha}}{12\mu} h_\sigma \frac{\partial P_0}{\partial \eta} \right) + \frac{\Omega R}{2} h_\sigma\, \eta_x \tag{18c}$$

where $\vec{\boldsymbol{\eta}}$ is the normal vector to the boundary (Γ^e) of an element. Note that Eq. (18*a*) includes the temporal fluid inertia term.

The integrals in Eqs. (16)–(18) are evaluated numerically over a master isoparametric element ($\hat{\Omega}$). Reddy and Gartling [18] detail the coordinate transformation and numerical integration procedure using Gauss-Legendre quadrature formulas. Eqs. (15) and (17), for each element of the flow domain, are assembled to form a linear system of equations represented as

$$\mathbf{K_G}\ \bar{\mathbf{P}}_{\mathbf{0_G}} = \mathbf{Q_{0_G}} + \mathbf{F_{0_G}} \tag{19a}$$

$$\mathbf{K_G}\ \bar{\mathbf{P}}_{\sigma_\mathbf{G}} = \mathbf{Q}_{\sigma\mathbf{G}} + \mathbf{F}_{\sigma\mathbf{G}} + \mathbf{S}_{\sigma_\mathbf{G}}\, \bar{\mathbf{P}}_{\mathbf{0_G}},^{\sigma=X,Y} \tag{19b}$$

where

$$\mathbf{K_G} = \bigcup_{e=1}^{Nem} \mathbf{k^e}, \quad \mathbf{Q}_{\sigma_\mathbf{G}} = \bigcup_{e=1}^{Nem} \mathbf{q}^\mathbf{e}_\sigma, \quad \mathbf{F}_{\gamma_\mathbf{G}} = \bigcup_{e=1}^{Nem} \mathbf{f}^\mathbf{e}_\sigma \ {}_{\sigma=0,X,Y} \tag{20}$$

The resulting global fluidity matrix $\mathbf{K_G}$ is symmetric and can be easily decomposed into its upper and lower triangular form, i.e.,

$$\mathbf{K_G} = \mathbf{L_G}\,\mathbf{L_G^T} \tag{21}$$

Boundary Conditions. Both the zero$_{\text{th}}$ and first order pressures are periodic in the circumferential direction,

$$\bar{P}_\gamma(\theta, z) = \bar{P}_\gamma(\theta + 2\pi, z), \quad {}_{\gamma;=0,X,Y} \tag{22}$$

The fluid pressure must be greater than the lubricant cavitation pressure (P_{cav}). For simplicity[3], the Gumbel condition of oil cavitation is enforced for the zero$_{\text{th}}$ and first order pressure fields. Note that Eqs. (15) and (17), for example, automatically satisfy the flow continuity at the boundary between a smooth land and groove. Hence, no special considerations in regard to flow matching are required. Other boundary conditions for the pressures are:

(a) Uniform pressure at the inlet plane ($z=0$),

$$\bar{P}^e_0\big|_{z=L} = P_{\text{supply}} \tag{23}$$

(b) Uniform pressure at exit plane ($z=L$),

$$\bar{P}^e_0\big|_{z=0} = P_{\text{exit}} \text{ and } \bar{P}^e_\sigma\big|_{z=L} = 0 \tag{24}$$

(c) At the inlet plane ($z=0$), the axial flow induced by the dynamic motion (fluid squeezing) is set to zero due to axial symmetry,

$$q_z\big|_{z=0} = 0 \tag{25}$$

This boundary condition implies that the perturbed axial flow does not cross the middle plane; hence there is a nonzero dynamic pressure field at this plane.

Once the $\mathbf{L}$ matrix and vectors $\mathbf{F_G}$ and $\mathbf{S_G}$ are obtained, and enforcing the boundary conditions at the inlet and exit planes of the flow domain, a process of back- and forward-substitutions renders the discrete zero$_{\text{th}}$ order pressure field $\bar{\mathbf{P}}_{0_G}$. Using the same fluidity matrix ($\mathbf{K_G}$) and the equilibrium pressure field, the first order pressure fields, $(\bar{\mathbf{P}}_\mathbf{X}, \bar{\mathbf{P}}_\mathbf{Y})_\mathbf{G}$, follow from Eq. (19*b*).

Effective Groove Depth. As advanced in Ref. [13], the laminar flow pattern at the groove is characterized by a recirculation region and a thru flow region. These regions are divided by a stream line that is considered to act as a physical boundary. Figure 5 shows a representation of the streamlines pattern for a pressure driven flow through a (symmetric) annular cavity with a supply groove and two mid-land grooves. The figure also depicts a close-up of CFD simulations of the pressure driven flow at the mid-land groove for two groove depths (10*c* and 15*c*). In this configuration the flow pattern at the supply and mid-land grooves is characterized by two regions, a recirculation region and a thru flow region. Furthermore, the dividing streamlines for the 10*c* and 15*c* groove depths present a similar penetration depth. In the proposed analysis, the streamlines dividing the two flow regions act as *physical boundaries* delimiting the domain for the flow induced due to dynamic (fluid squeezing) journal motions. Thus, the fluid film clearance at the groove is represented in terms of an effective clearance $c_\eta = (d_\eta + c)$, with d_η as an effective groove depth and c as the clearance of the smooth land.

Model Predictions and Validation To Test Data

This section presents comparisons of experimental and predicted damping, stiffness and mass coefficients for the oil ring seal described in Ref. [7]. Figure 6 depicts the actual dimensions of the test seal, and Table 1 lists the seal physical dimensions, fluid properties and operating conditions.

As in the tests[4], the analysis reports predictions for half of the axially symmetric grooved seal configuration. Published test data and predictions follow for a smooth land seal and one with an inner groove 15*c* in depth. The effective central groove depth equals 9*c* and the inner land groove depth is set to 6*c*. Note the selected parameters are greatly different from the actual physical magnitudes [13].

Figure 7 shows the seal reaction forces versus the static journal eccentricity. Predictions and experimental results present good correlation for journal eccentricities up to $e/c = 0.5$ for the grooved and smooth seals. For the largest journal eccentricity ($e/c = 0.7$), predictions are within 20% of the experimental results for the smooth seal. On the other hand, the reaction force of the grooved seal is underpredicted by a factor of 2 for the highest journal eccentricity. For the largest journal eccentricities the oil temperature is expected to significantly increase due to the small film thickness (i.e. large shear forces and power loss). Thus, the actual seal clearance and oil properties for the largest eccentricity may differ significantly from the nominal values, thus having a large uncertainty. Ref. [7] does not detail information on the exit temperature or measurements of *hot* clearances (immediately after testing). Hence, further predictions are compared with test data for journal eccentricities in the low to mid-range, i.e., $\varepsilon = 0$, 0.3, 0.5 only.

Figures 8 and 9 depict the direct and crossed-coupled stiffness coefficients (K) versus the operating journal eccentricity, respectively. The predictions correlate well with the test data for the lower journal eccentricity ratios ($\varepsilon = 0$, 0.3). For the 50%

[3]The omission of a physically sound model for lubricant cavitation (vapor or gas) is not grave. Oil seals with their large pressure differentials rarely develop pressures below ambient. Open ends SFDs; on the other hand, are subject more to air entrainment than lubricant cavitation.

[4]The experimental force coefficients reported equal to 50% of the measured values for the whole test arangement configuration, i.e., two seals in parallel.

Downloaded 16 Aug 2012 to 165.91.101.108. Redistribution subject to ASME license or copyright; see http://www.asme.org/terms/Terms_Use.cfm

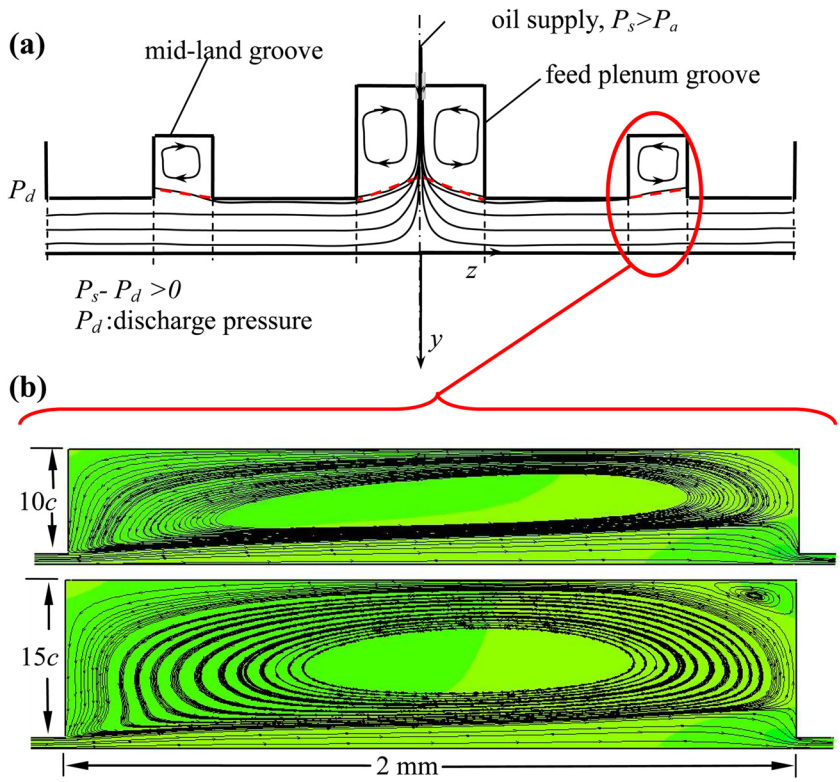

Fig. 5 (*a*) Schematic view of streamlines in axially symmetric grooved annular cavity ($\Delta P = P_s - P_d$). (*b*) CFD simulation of pressure driven streamlines across a 10*c* and 15*c* circumferential mid-land groove in an oil seal tested in Ref. [7]. ($c = 86$ mm, Ω=10,000 rpm, D = 117 mm.)

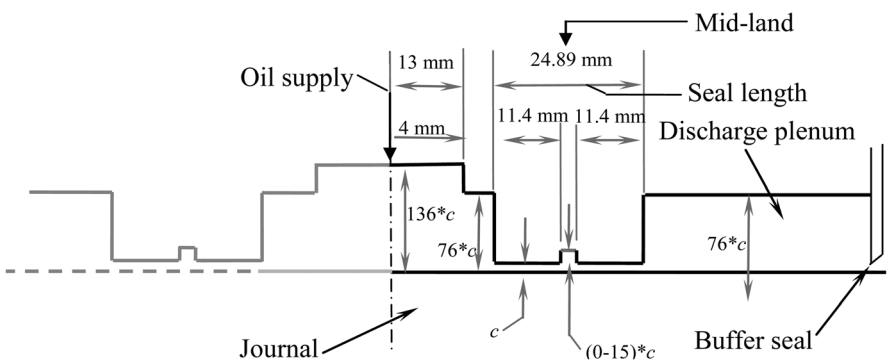

Fig. 6 Schematic view and dimensions of test (parallel) oil seal in Refs. [6,7]

Table 1 Test oil seal configuration, operating conditions fluid properties, Refs. [6,7]

Dimensions	
Diameter, 2*R*	117 mm
Land length	24.89 mm
Radial land clearance, *c*	85.9 μm
Central groove length	17 mm
Central groove depth	136*c*
Inner land groove length	2 mm
Inner land groove depth	0*c* and 15*c*
Operating parameters and oil	
Shaft speed, Ω	4,000-10,000 rpm
Supply pressure	70 bar
Static journal eccentricity (e_0/c)	0.0-0.7
Oil density, ρ	850 kg/m^3
viscosity (smooth seal), μ	0.016 Pa.s (54 °C)
viscosity (grooved seal)	0.019 Pa.s (49 °C)

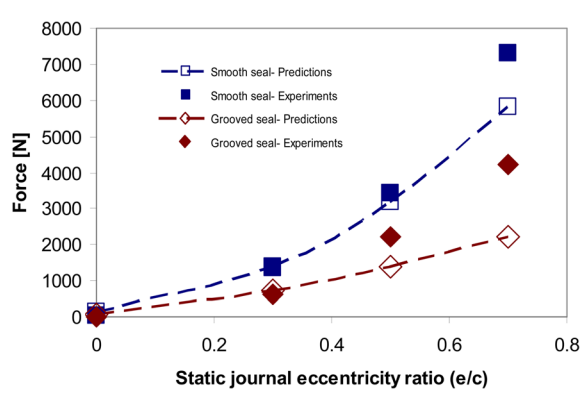

Fig. 7 Predicted reaction forces for smooth seal and seal with inner land groove ($c_\eta = 7c$) versus journal eccentricity ratio. Experimental data for smooth seal and seal with inner land groove ($c_g = 15c$), 10,000 rpm, 70 bar [7].

Downloaded 16 Aug 2012 to 165.91.101.108. Redistribution subject to ASME license or copyright; see http://www.asme.org/terms/Terms_Use.cfm

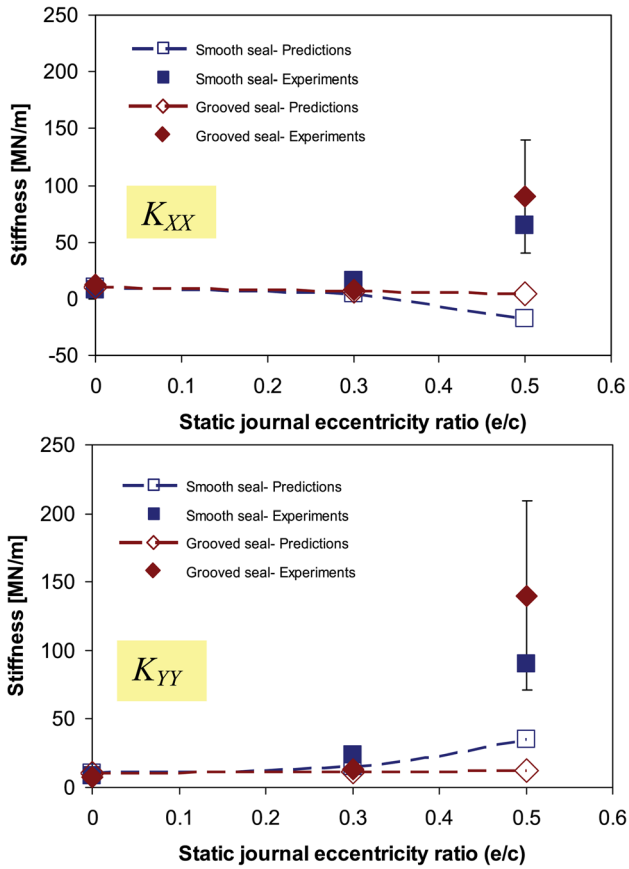

Fig. 8 Predicted seal direct stiffness coefficient (K_{XX}, K_{YY}) versus journal eccentricity ratio. Experimental data for smooth seal and seal with inner land groove ($c_g = 15c$), 10,000 rpm, 70 bar [7].

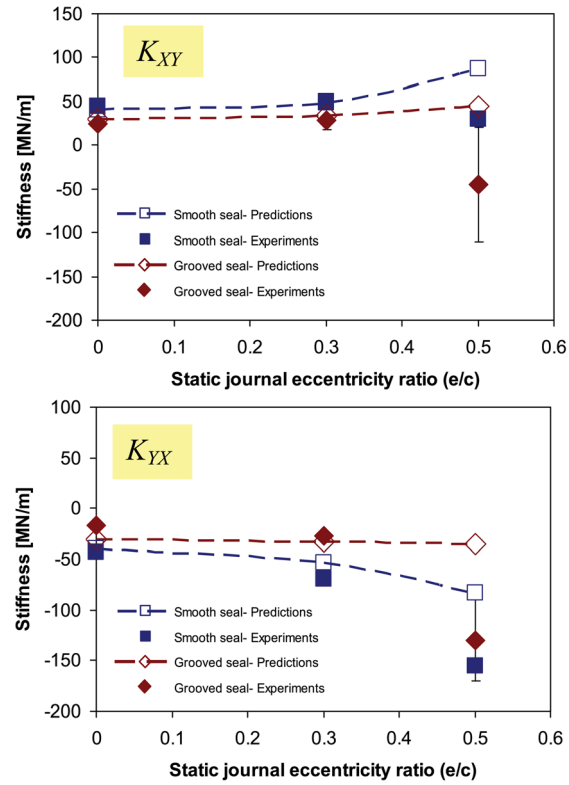

Fig. 9 Predicted cross-coupled stiffness coefficients (K_{XY}, K_{YX}) versus journal eccentricity ratio. Experimental data for smooth seal and seal with inner land groove ($c_g = 15c$), 10,000 rpm, 70 bar [7].

eccentricity ratio there are discrepancies. The differences can be attributed in part to the lack of knowledge in actual clearance and oil exit temperature, not reported in Ref. [7].

Figure 10 depicts the cross-coupled stiffness coefficients versus journal speed for two eccentricities ($e/c = 0, 0.3$). The predictions are in good correlation with the experimental results. In particular, the model adequately predicts the reduction of the cross-coupled coefficients after adding the inner groove into the (original) smooth land seal.

Figures 11 and 12 present the direct and cross-coupled damping coefficients (C) versus static journal eccentricity ratio, respectively. The direct damping coefficients (C_{XX}, C_{YY}) show excellent correlation for the most eccentricities, except for the C_{XX} coefficient of the smooth seal that is 20% underpredicted at $e/c = 0.5$. The cross-coupled coefficients are much smaller than the direct damping coefficients, showing a moderate to good correlation with the test data for the various journal eccentricities.

Figure 13 depicts the direct added mass coefficients (M) versus journal eccentricity. Predicted and experimental cross-coupled added mass coefficients (M_{XY}, M_{YX}) are nearly null and not shown. The direct added mass coefficients (M_{XX}, M_{YY}) are in good agreement with the experimental data. In particular, the analysis predicts a larger added mass coefficient for the grooved oil seal as the experiments also reveal. Note that the predicted added mass coefficient is nearly constant for all journal eccentricities. For comparison, the graph includes the predicted mass coefficient obtained using the classical formula in Ref. [12], valid for a smooth land configuration with ambient pressure at its ends.

Figure 14 depicts the seal leakage versus static journal eccentricity for operation at 10,000 rpm and 70 bar feed pressure. There is good correlation between experiments and predictions with a variation of less than ~15% for both seals, hence the selected

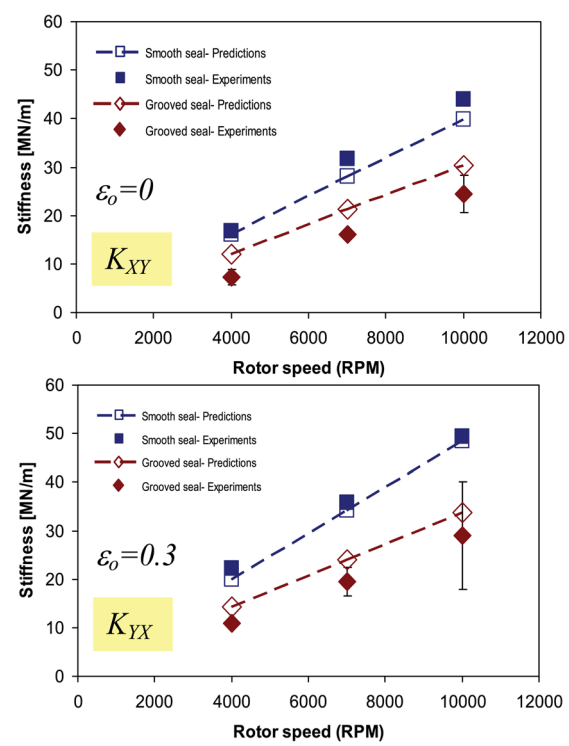

Fig. 10 Predicted cross-coupled stiffnesses (K_{XY}, K_{YX}) versus shaft speed at two journal eccentricities (0, 0.3). Experimental data for smooth seal and seal with inner land groove ($c_g = 15c$), 10,000 rpm, 70 bar [7].

Downloaded 16 Aug 2012 to 165.91.101.108. Redistribution subject to ASME license or copyright; see http://www.asme.org/terms/Terms_Use.cfm

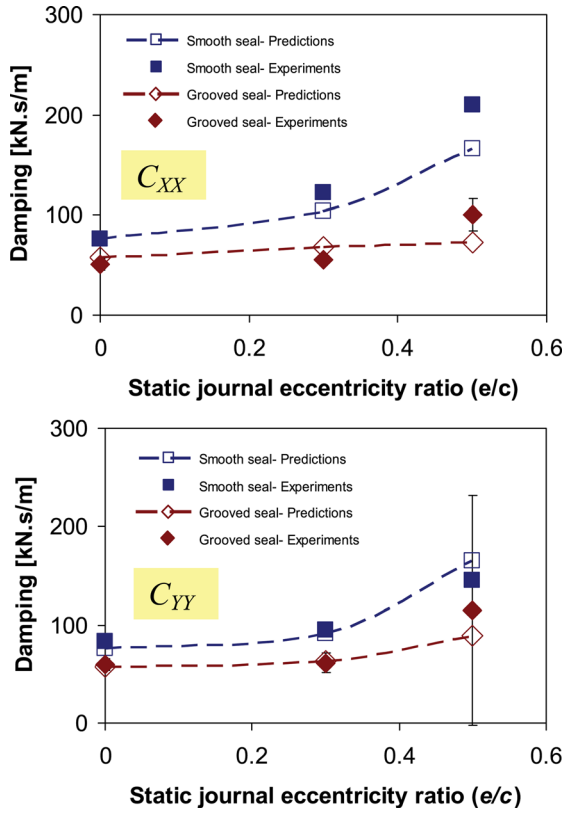

Fig. 11 Predicted direct damping coefficients (C_{XX}, C_{YY}) versus journal eccentricity ratio. Experimental data for smooth seal and seal with inner land groove ($c_g = 15c$), 10,000 rpm, 70 bar [7].

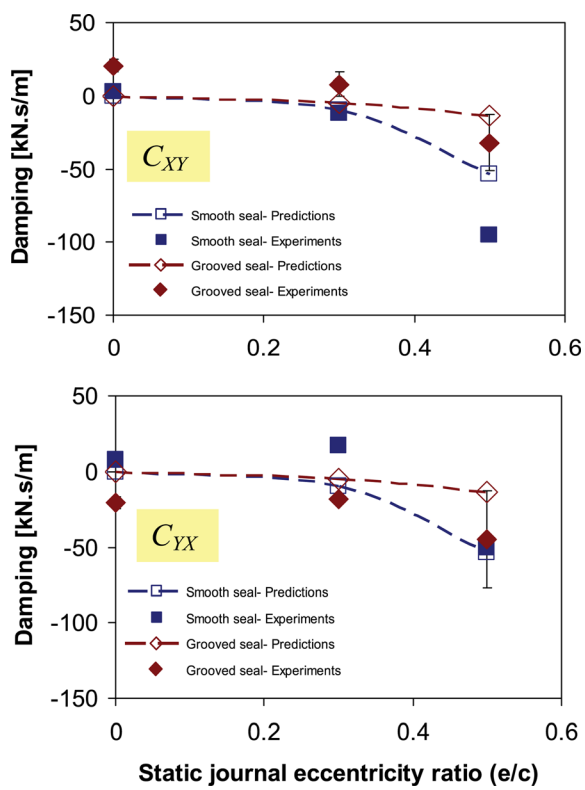

Fig. 12 Predicted cross-coupled damping coefficients (C_{XY}, C_{YX}) versus journal eccentricity ratio. Experimental data for smooth seal and seal with inner land groove ($c_g = 15c$), 10,000 rpm, 70 bar [7].

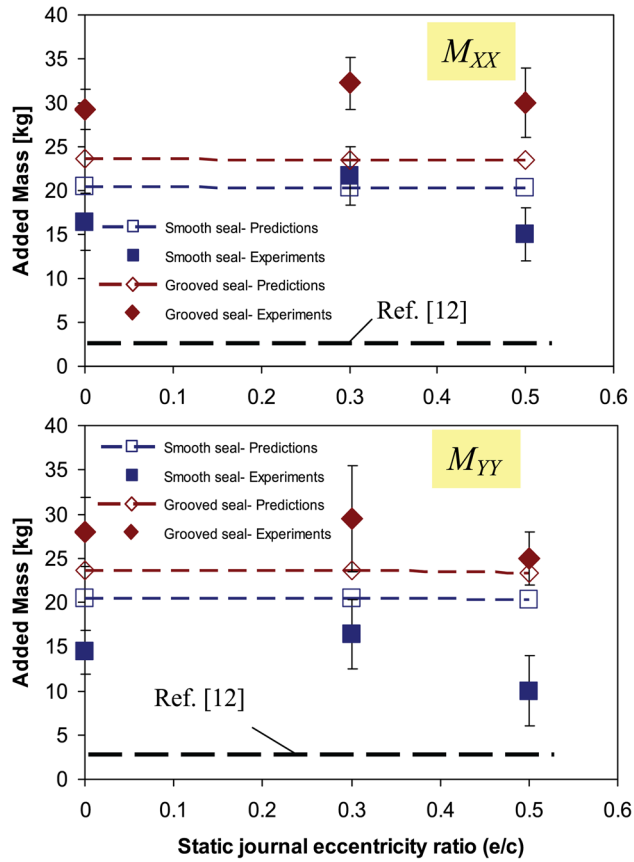

Fig. 13 Predicted added mass coefficient (M_{XX}, M_{YY}) versus journal eccentricity ratio. Experimental data for smooth seal and seal with inner land groove ($c_g = 15c$), 10,000 rpm, 70 bar [7].

effective groove depth represents the physical boundaries of the axial through flow very well. Note that the experiments and predictions show that the smooth seal leaks more than the grooved seal because its effective viscosity is slightly lower and its land clearance larger, hence there are larger power losses inducing a lubricant temperature rise.

For completeness, Appendix A shows predicted pressure fields in the seal land and grooved regions (central plenum and inner land) that make evident the fluid inertia character of the pressures in the grooved regions and their influence extending into the film lands of the seal.

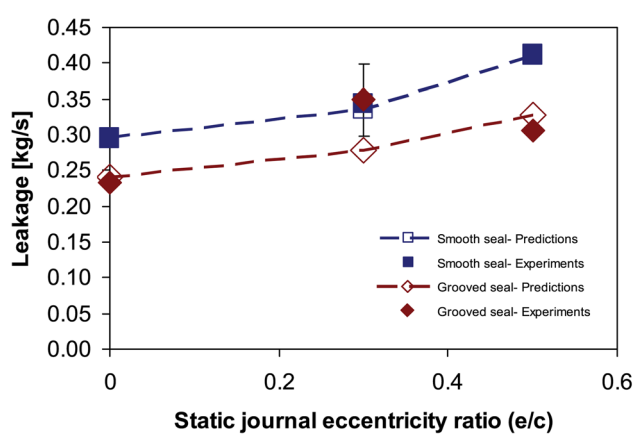

Fig. 14 Seal leakage versus journal eccentricity ratio: predictions and test data for smooth seal and seal with inner land groove ($c_g = 15c$), 10,000 rpm, 70 bar [7]

Downloaded 16 Aug 2012 to 165.91.101.108. Redistribution subject to ASME license or copyright; see http://www.asme.org/terms/Terms_Use.cfm

Conclusions

This paper presents a bulk-flow formulation to obtain fluid film forces developed in grooved oil seals and details the implementation of a finite element method to obtain the force coefficient for journal off-centered operation. The current analysis extends an original bulk-flow model [13] developed for small amplitude journal motions about a *centered* position. The present analysis also predicts added mass coefficients, largely ignored in previous analyses of laminar-flow oil seals.

The force coefficients, leakage and reaction forces of a smooth and grooved oil seal are predicted and compared to experimental results reported in Ref. [7]. The test grooved oil seal includes a rectangular central groove located at the seal mid-land plane with a depth of 15 times the seal clearance ($c = 85.9$ μm). The predicted parameters are compared to experimental results for four journal eccentricities ($e/c = 0$, 0.3, 0.5, 0.7) at 10,000 rpm and with a 70 bar oil feed pressure.

Predicted and experimental force coefficients present good correlation for the direct force coefficients for the lower journal eccentricities ($e/c = 0$,0.3) and moderate to good correlation for $e/c = 0.5$. The cross-coupled stiffness coefficients are also accurately predicted for the lower journal eccentricities. In particular, the current model accurately predicts the reduction of the direct stiffness, direct damping, and cross-coupled stiffness coefficients when adding a circumferential groove to the seal land. The added mass coefficients for both seals are also predicted accurately (within 20%). Furthermore, the analysis and experimental results indicate that a grooved seal shows larger direct added mass coefficient than a smooth seal.

For journal eccentricity ratios (e/c) up to 70%, there are discrepancies between the experimental results and (current) predictions for some of the force coefficients. These discrepancies are attributed to (unknown) changes in seal clearance and oil viscosity induced by thermal effects when operating at large static eccentricities. Regrettably, Ref. [7] does not offer enough details on operating conditions and the variation of the lubricant properties and seal clearance with temperature. Therefore, the predictions are compared with experimental results only for the low to mid-range of journal eccentricities ($\varepsilon = 0$, 0.3, 0.5).

The presented analysis represents a significant improvement over prevailing predictive tools to analyze grooved oil seals. More importantly, accurate predictions of grooved oil seal force coefficients can lead to improved estimations of rotordynamic instability thresholds in centrifugal compressors.

Acknowledgment

The support of the TAMU Turbomachinery Research Consortium is gratefully acknowledged.

Nomenclature

C_{ij} = seal damping coefficients [N.s/m] $i, j = X,Y$
c = seal land clearance [m]
$c_\eta = c + d_\eta$. clearance at groove [m]
d_η = effective groove depth [m]
e_0 = journal static eccentricity [m]
h = film thickness [m]
F_i = sea reaction forces [N], $i = X,Y$
L = axial length [m]
K_{ij} = seal stiffness coefficients [N/m] $i,j = X,Y$
M_{ij} = seal added mass coefficients [kg] $i,j = X,Y$
$\dot{m}_x$, $\dot{m}_z$ = mass flow rates, circumferential & axial [kg/s]
N = number of sub-regions in flow domain
N_{em} = number of elements (FEM mesh)
n_{pe} = number of Nodes per element (FEM mesh)
P = pressure [Pa]
P_X, P_Y = first-order pressure fields [Pa/m]
q_x, q_z = volumetric flow rates/unit length [m^2/s]
i = imaginary unit ($\sqrt{-1}$)
R = journal radius [m]
$\overline{\mathrm{Re}}_* = \rho\omega c_\eta^2/12\mu$ modified squeeze film Reynolds number
t = time [s]
V_x, V_z = bulk flow velocities [m/s]
X,Y,Z = inertial coordinate system [m]
x, z = circumferential and axial coordinates [m]
Δe = journal dynamic amplitude of motion [m]
$\varepsilon = e_0/c$, journal eccentricity ratio
μ = lubricant viscosity [Pa.s]
Ω = journal rotational speed [rad/s]
ω = whirl frequency [rad/s]
ρ = lubricant density [kg/m^3]
$\theta = x/R$, angular coordinate [deg]
ψ = finite element interpolation functions

Vectors and Matrices

$\mathbf{k^e}, \mathbf{K_G}$ = fluidity matrices, element & global
$\mathbf{q^e}, \mathbf{Q_G}$ = nodal flow rate vectors, element & global
$\mathbf{f^e}, \mathbf{F_G}$ = shear & squeeze flow rate vectors, element & global

Subscripts

d = discharge
g = groove
N = last annular cavity section
s = supply

Appendix: A Note on Dynamic Pressures Generated in Grooved Seals

Predictions for the dynamic pressure field generated in the seal lands and feed central plenum due to small amplitude journal motion about a centered position follow. These results serve to illustrate the inertial nature of the pressure field in the grooved

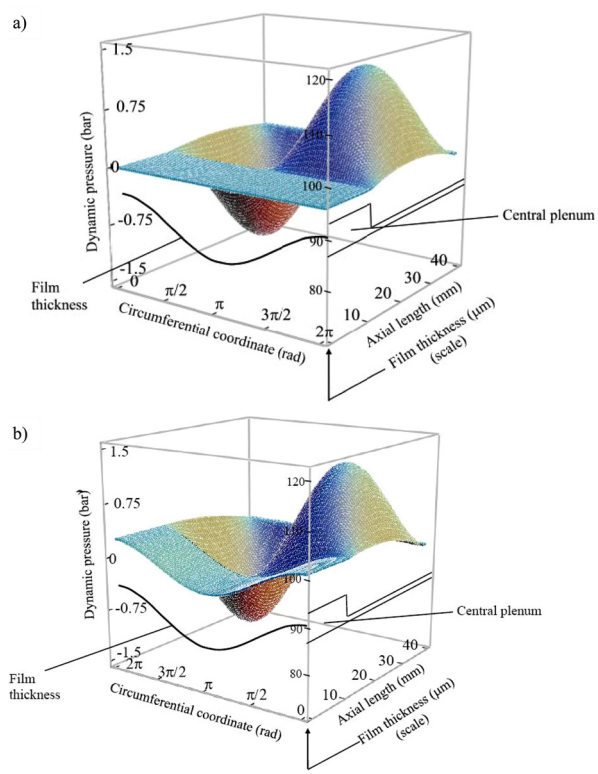

Fig. 15 Predicted dynamic pressure fields in seal due to journal whirl motions (5 μm, $\omega = 200$ Hz). (*a*) Classical theory [12] assumes null dynamic pressure in deep plenum; (*b*) Current model with effective central plenum clearance ($c_{\eta_l} = 12c$). Film thickness noted.

Downloaded 16 Aug 2012 to 165.91.101.108. Redistribution subject to ASME license or copyright; see http://www.asme.org/terms/Terms_Use.cfm

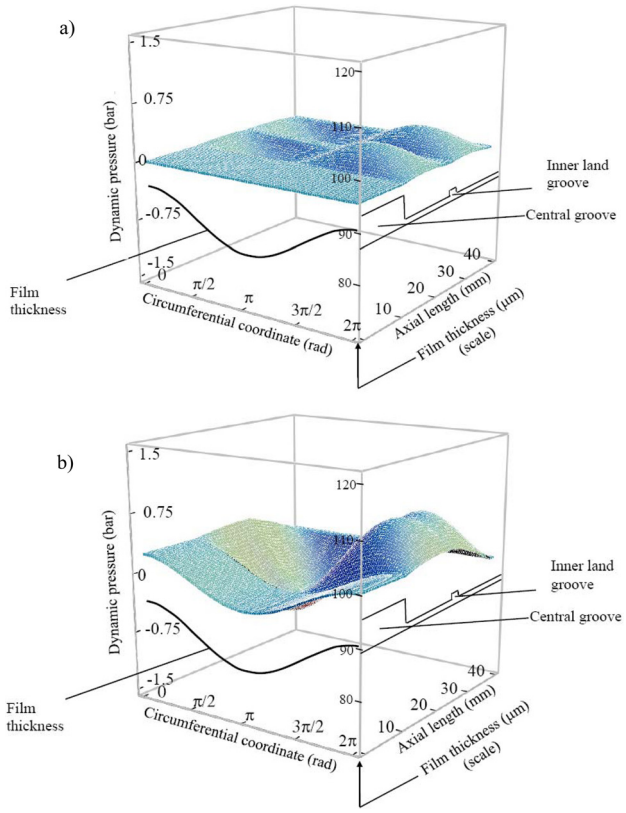

Fig. 16 Predicted dynamic pressure fields in seal with inner land groove due to journal motions (5 μm, $\omega = 200$ Hz). (*a*) Classical theory [12] assumes null dynamic pressure in deep plenum and inner groove; (*b*) Current model with effective plenum and inner groove clearances ($c_{\eta_I} = 12c$, $c_{\eta_{III}} = 7c$).

regions and their effect on the pressure in the seal lands. Note that the pressure field is a function of both the time and the circumferential coordinate; however, for circular centered orbits, the pressure is stationary in a coordinate system rotating with the journal center precessional speed [16].

For a supply pressure of 70 bar, Fig. 15 shows the dynamic pressure field for the smooth land parallel seals with a 5 μm whirl amplitude and 200 Hz frequency and journal spinning at 10,000 RPM. Figure 15(*a*) depicts the dynamic pressure assuming a null dynamic pressure generation at the central plenum, while Fig. 16(*b*) depicts the pressure field accounting for an effective plenum clearance ($c_{\eta_I} = 12c$). Note that the pressure at the groove is mainly due to fluid inertia effects as it is 180^0 out of phase with respect to the acceleration of the film thickness (d^2h/dt^2). Furthermore, although the peak dynamic pressure in the seal film land (due to viscous effects) is similar to that shown in Fig. 15(*a*), Fig. 15(*b*) shows that the influence of the inertial pressure field generated at the groove extends to the film land and amplifies the fluid inertia effect (radial force) over the entire axial length of the seal land.

Figures 16 shows predicted dynamic pressure fields for the seal with the deepest inner land groove ($c_{III} = 15c$). The pressure field also corresponds to small journal motions about a centered position (10 μm, 200 Hz). Figure 16(*a*) depicts the pressure field assuming both the central plenum and inner land groove do not generate dynamic pressures, i.e., infinitely deep. Note that the peak pressure in the seal land is much smaller (around 1/4) than that of the smooth land seal. This pressure profile yields direct damping and added mass coefficients smaller by a factor 2 and 5 with respect to the test data in Ref. [7], respectively.

Figure 16(*b*) shows the pressure field using an effective central plenum (c_{η_I}) and inner land ($c_{\eta_{III}}$) groove clearance of 12c and 7c, respectively. In this case, both the plenum and inner-land groove enhance fluid inertia effects along the seal lands. In fact, as the experimental results show, the added mass coefficients identified from the grooved seal (~30 kg) are larger than those associated to the smooth land seal (~20 kg).

References

[1] Childs, D. W., Rodriguez, L. E., Cullotta, V., Al-Ghasem, A., and Graviss, M., 2006, "Rotordynamic-Coefficients and Static (Equilibrium Loci and Leakage) Characteristics for Short, Laminar-Flow Annular Seals," ASME J. Tribol. **128**(2), pp. 378–387.

[2] Kirk, R., 1986, "Oil Seal Dynamic Considerations for Analysis of Centrifugal Compressors," *Proc. 15th Turbomachinery Symposium*, Houston, TX, pp. 25–34.

[3] Semanate, J., and San Andrés, L., 1993, "Analysis of Multi-Land High Pressure Oil Seals," STLE Tribol. Trans. **36**(4), pp. 661–669.

[4] Baheti, S. and Kirk, R., 1995, "Finite Element Thermo-Hydrodynamic Solution of Floating Ring Seals for High Pressure Compressors Using the Finite-Element Method," STLE Tribol. Trans., **38**, pp. 86–97.

[5] Allaire, P. E., and Kocur, J. A. Jr., 1985, "Oil Seal Effects and Subsynchronous Vibrations in High-Speed Compressors," Proc. Symposium on Instability in Rotating Machinery, Carson City, Nevada, June 10–14, NASA Conf. Publ. 2409, pp. 205–223.

[6] Childs, D. W., Graviss, M., and Rodriguez, L. E., 2007, "The Influence of Groove Size on the Static and Rotordynamic Characteristics of Short, Laminar-Flow Annular Seals," ASME J. Tribol. **129**(2), pp. 398–406.

[7] Graviss, M., 2005, "The Influence of a Central Groove on Static and Dynamic Characteristics of an Annular Liquid Seal with Laminar Flow," M.S. thesis, Texas A&M University, College Station, TX.

[8] Childs, D. W., 1993, *Turbomachinery Rotordynamics*, John Wiley & Sons, New York, Chap. 3.

[9] Wilcox, E., 1999, "Unexpected Rotordynamic Instability in a 'Proven' FCC Wet Gas Compressor," *Proc. of the 28th Turbomachinery Symposium*, Texas A&M University, Houston (September), **28**, pp. 41–49.

[10] Kaneko, S., Hori, Y., and Tanaka, M., 1984, "Static and Dynamic Characteristics of Annular Plain Seals," *Proc. Third IMechE Int. Conf. Vibrations in Rotating Machinery*, York, England, pp. 205–214.

[11] Zirkelback, N., and San Andrés, L., 1996, "Bulk-Flow Model for the Transition to Turbulence Regime in Annular Seals," STLE Tribol. Trans., **39**(4), pp. 835–842.

[12] Reinhardt, F., and Lund, J. W., 1975, "The Influence of Fluid Inertia on the Dynamic Properties of Journal Bearings," ASME J. Lubr. Technol., **97**(1), pp. 154–167.

[13] Delgado, A., and San Andrés, L., 2010, "A Model for Improved Prediction of Force Coefficients in Grooved Squeeze Film Dampers and Oil Seal Rings," ASME J. Tribol., **132** (3), 032202.

[14] Gehannin, J., Arghir, M., and Bonneau O., 2010, "Complete Squeeze-Film Damper Analysis Based on the 'Bulk Flow' Equations," STLE Tribol. Trans., **53**, pp. 84–96.

[15] Arghir, M., and Frene, J., 2004, "A Bulk-flow Analysis of Static and Dynamic Characteristics of Eccentric Circumferentially-Grooved Liquid Annular Seals," ASME J. Tribol. **126**(2), pp. 316–326.

[16] San Andrés, L., and Vance, J., 1986, "Effect of Fluid Inertia on Squeeze-Film Damper Forces for Small-Amplitude Circular-Centered Motions," ASLE Trans. **30**(1), pp. 63–68.

[17] San Andrés, L., 2009, "Thermal Analysis of Finite Length Journal Bearings Including Fluid Inertia, Modern Lubrication Theory," Notes 7, Texas A&M University, Virtual Library System, https://repository.tamu.edu/handle/1969.1/93197

[18] Reddy, J. N., and Gartling, D. K., 2001, *The Finite Element Method in Heat Transfer and Fluid Dynamics*, CRC Press, Boca Raton, FL, Chap. 2.

Downloaded 16 Aug 2012 to 165.91.101.108. Redistribution subject to ASME license or copyright; see http://www.asme.org/terms/Terms_Use.cfm